Nonlinear Interactions between solitary waves and structures in a steady current

Y.F. Yang[a,b], Y.Q. Zheng[a], H. Ge[a,c], C.Z. Wang[a*, c]

[a]*Ocean College, Zhejiang University, Zhoushan, 316021, China*

[b]*Department of Mechanical Engineering, University College London, Torrington Place, London WC1E 7JE, UK*

[c]*Yangjiang Offshore Wind Power Laboratory, Yangjiang, 529500, China*

Abstract

Interactions between solitary waves and structures in a steady current are studied based on a fully nonlinear wave potential theory, and a higher order finite element method (FEM) with a mesh of 8-node quadrilateral isoperimetric elements is employed to simulate the interaction in two-dimensions. Numerical examples are given by solitary waves propagating over an underwater rectangular cylinder in a steady current in a tank and solitary waves acting on single- and twin-rectangular cylinders in a steady current on free surface. Waves and hydrodynamic forces are obtained at different current speeds. It is found that the peak of diffracted wave due to the first and second reflections by an underwater cylinder clearly increase in following current. Furthermore, a packet of periodic waves with constant peak and trough are found to appear when the absolute value of the Froude number becomes large enough in single- and twin-cylinder cases. For the twin-cylinder cases, the maximum wave and horizontal force are clearly affected by the current especially in larger incident wave amplitudes and smaller spacings. In addition, the nonlinearity of wave or force becomes stronger at larger Froude numbers and larger incident wave amplitudes.

Key Words: Solitary wave; current; nonlinear interaction; potential flow theory; higher order finite element method.

1. Introduction

The solitary wave is one typical nonlinear wave in ocean, which normally appears on the ocean surface in the coastal region. In ocean engineering and naval architecture, we normally consider the hydrodynamic properties of the designed offshore structures in such types of water waves. In reality, water waves and currents always coexist in ocean. In such a case, the hydrodynamic properties of offshore structures may be quite different when compared with the

cases without the currents. Thus, it is of great importance to consider the problem of a solitary wave interaction with structures in a steady current.

Solitary wave propagation in shallow water and its interactions with coastal structures received extensive attention in the past decades. One important research topic is solitary wave propagation in ocean or in sloping beaches and quite a lot studies can be found. Typical numerical examples including Kim et al. (1983) and Maiti and Sen (1999) by using a boundary element method, and Synolakis (1987) by applying Carrier & Greenspan transformation (Carrier and Greenspan, 1958), and Knowles and Yeh (2018) through higher-order pseudo-spectral method. Besides, another interesting problem is the collision between two and multiple solitary waves. For example, Su and Mirie (1980) and Mirie and Su (1982) studied the two-dimensional interactions between two solitary waves by perturbation theory. Later the similar problem is investigated by Cooker et al. (1997) and Chambarel et al. (2009) through the boundary element method. Moreover, works about three-dimensional interaction between two equal steep solitary waves or the obliquely reflection of a solitary wave can be found in Miles (1977), Tanaka (1993) and Kodama and Yeh (2016), they found that the three-dimensional interactions between solitary waves are very complicated, the Mach reflection phenomenon will occur during the interaction. In addition to the analytical and numerical works above, typical experimental studies including Seabra-Santos et al. (1987) and Chen et al. (2015).

For practical consideration, it is also important to consider the interaction between solitary waves and offshore structures. Sibley et al. (1982) analyzed the forces of a solitary wave on a fixed two-dimensional cylinder by an approximated approach. Later, this diffraction problem is investigated numerically by Chian and Ertekin (1992) through the boundary element method. A similar method is also employed by Cao et al. (1993) to study the two-dimensional solitary waves generated by a moving disturbance beneath the water surface. A more recent work by Sun et al. (2015) considered the fully nonlinear interactions between a solitary wave and two-dimensional structures floating on free surface based on a higher order finite element method. Various cases of the forces by solitary wave acting on a single- or twin-cylinder rectangular cylinder on free surface are simulated and the effect of wave amplitude, initial draught and breadth of cylinder on waves and hydrodynamics forces have been discussed. For three-dimensional problems, Isaacson (1982) proposed a three-dimensional fully nonlinear boundary element method to analyze the interaction between a solitary wave and fixed or floating bodies. Based on the generalized Boussinesq equations, Wang et al. (1992) considered the diffraction of a solitary wave by a vertical circular cylinder, their results are further verified by experiments later in Yates and Wang (1994). Using the same equations, Wang and Jiang (1993) and Zhao et al. (2007) extended it to the diffraction of a solitary wave by an array of circular cylinders, such as two and four groups of cylinders. Based on the fully nonlinear velocity potential theory, Zhou et al. (2015)

considered the interactions between a solitary wave and a fixed or a floating circular cylinder, the wave forces on both cases are compared and discussed in detail. Besides, the first-order, third-order and fully nonlinear initial conditions are also applied and analyzed in their work.

In the real ocean environment, wave and current always coexist. The wave-current interaction has been one of the most interesting, applicable topics in naval architecture and ocean engineering. Compared with the cases only water wave exists, wave loads on these ships and offshore structures and the corresponding wave run-ups will be significantly affected when wave and current coexist. Thus, it is of practical importance to consider the interaction between wave-current and structures theoretically. In the last two decades, the fully nonlinear potential flow model was used to simulate interaction problems of periodic waves and structures in a current. For example, Celebi (2001) investigated the transient and steady-state nonlinear wave–current-body interactions by using a fully nonlinear three-dimensional numerical wave tank with a mixed Eulerian–Lagrangian time stepping technique. Ryu et al. (2003) developed a two-dimensional boundary element based numerical wave tank to investigate two-dimensional wave-current interactions. They found that wave crests, troughs, and wavelength changed due to wave–current interactions. Wang et al. (2018) developed an enhanced spectral boundary integral method to study the full nonlinear three-dimensional wave and current interaction.

As far as we know, there is little work about the interactions between a solitary wave and a structure in a current. Some works are about solitary wave and current interactions only. Zhang et al. (2015) used a RANS equations based VOF (volume of fluid) method to simulate a solitary wave traveling in a steady current. They found that the solitary wave becomes smaller in wave height and larger in wave width when the current advanced in the same direction as the wave propagates. On the contrary, they become larger and smaller, respectively, which is similar to the interaction between a periodic wave with a current. However, their work does not consider the wave interaction with a structure in a current. Cheng et al. (2020) considered the solitary wave slamming on an oscillating wave surge converter under the effects of a uniform current by a higher-order boundary element method. In the present paper, the fully nonlinear interactions between solitary waves with structures in a uniform current are studied based on a higher order finite element method. The problem without the current effect was considered by one of the authors and co-workers in Sun et al. (2015) and it is extended to the cases with a uniform current in the present study, which mainly tries to figure out how the uniform current affect the wave and hydrodynamic force subjected by the structure. When there is an incident current, the incident component of the velocity potential here should be re-derived. Besides, the former procedure to calculate the hydrodynamic force should also be revised by including a term induced by the current. Compared with the former cases without the current, the wave elevation

and hydrodynamic forces on the structures may be deeply affected. The nonlinearity of the numerical results may also be different. To illustrate the influence of the current, case studies are conducted for solitary waves propagation over an underwater rectangular cylinder in a tank with a steady current and solitary wave acting with single- and twin-rectangular cylinders in a steady current on free surface.

2. Mathematical formulation

2.1 *Governing equation and boundary conditions*

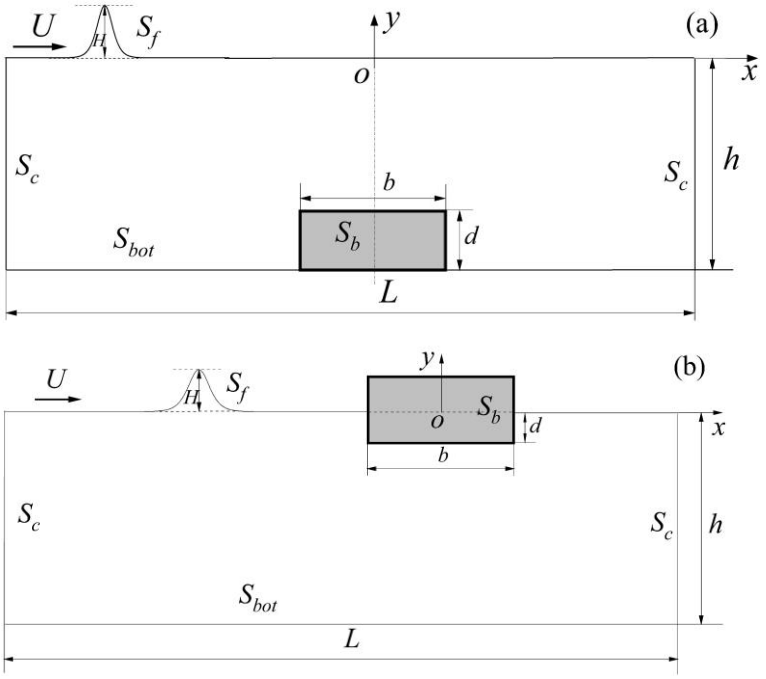

Fig. 1. A sketch of a solitary wave interactions with a body in a current；(a) An underwater and bottom-mounted rectangular cylinder; (b) A rectangular cylinder on free surface.

The problem of a solitary wave interaction with a two-dimensional structure is investigated in this article. Two different configurations are considered. The first is a submerged and bottom-mounted rectangular cylinder, and the second is a rectangular cylinder floating on free surface, as given in Fig. 1. A Cartesian coordinate system *O-xy* is defined as shown in Fig. 1, the origin is located at the vertical centre line of the structure, the *x*-axis coincides with the undisturbed free surface, and the *y*-axis points upwards. The free surface and the cylinder surface are denoted as S_f and S_b, respectively, and the unit normal vector is directed outward from the fluid region is denoted by $\vec{n} = (n_x, n_y)$.The bottom of the fluid is assumed to be a horizontal plane at *y*=-*h* and it is denoted by S_{bot}, the artificial boundaries S_c in the figure are located at *x*=0 and *x*=*L* for left and right edges, respectively. The fluid is assumed to be incompressible and inviscid, and

the motion of the fluid is irrotational. Thus, the liquid motion can be described through a velocity potential Φ, which satisfies the Laplace equation in the fluid domain $\forall$

$$\nabla^2\Phi = 0 \qquad \text{in} \quad \forall . \tag{1}$$

The Φ is subject to the following boundary conditions on the free surface S_f

$$\frac{\partial \eta}{\partial t} + \frac{\partial \Phi}{\partial x}\frac{\partial \eta}{\partial x} - \frac{\partial \Phi}{\partial y} = 0 \qquad \text{on } S_f , \tag{2}$$

$$\frac{\partial \Phi}{\partial t} + g\eta + \frac{1}{2}\left|\nabla\Phi\right|^2 = 0 \qquad \text{on } S_f , \tag{3}$$

where g is the acceleration due to gravity. The condition on the cylinder surface can be expressed as

$$\frac{\partial \Phi}{\partial n} = 0 \qquad \text{on } S_b , \tag{4}$$

On the tank bottom the boundary condition is

$$\frac{\partial \Phi}{\partial y} = 0 \qquad \text{on } \ y = -h \ . \tag{5}$$

In addition, the potential satisfies the radiation condition which is imposed through a suitable numerical procedure on S_c.

For a problem with a steady current with speed U along the x-axis, the velocity potential Φ may be split into two parts:

$$\Phi = \phi + Ux , \tag{6}$$

where ϕ is the disturbed potential and Ux is the potential due to the current. The potential ϕ also satisfies Laplace equation

$$\nabla^2\phi = 0 \qquad \text{in} \quad \forall \tag{7}$$

The boundary conditions mentioned above or Eqs. (2) ~ (5) may be expressed in terms of the disturbed potential ϕ as

$$\frac{\partial \eta}{\partial t} + \frac{\partial \phi}{\partial x}\frac{\partial \eta}{\partial x} - \frac{\partial \phi}{\partial y} + U\frac{\partial \eta}{\partial x} = 0 \qquad \text{on } S_f , \tag{8}$$

$$\frac{\partial \phi}{\partial t} + g\eta + \frac{1}{2}\left|\nabla\phi\right|^2 + U\frac{\partial \phi}{\partial x} = 0 \qquad \text{on } S_f \ , \tag{9}$$

$$\frac{\partial \phi}{\partial n} = -Un_x \qquad \text{on } \ S_b , \tag{10}$$

$$\frac{\partial \phi}{\partial y} = 0 \qquad \text{on } \ y = -h \ . \tag{11}$$

Eqs. (8) and (9) can be written in Lagrangian form

$$\frac{Dx}{Dt} = \frac{\partial \phi}{\partial x} + U , \frac{Dy}{Dt} = \frac{\partial \phi}{\partial y} , \tag{12}$$

$$\frac{D\phi}{Dt} = -g\eta + \frac{1}{2}\left|\nabla\phi\right|^2, \tag{13}$$

where $\frac{D}{Dt} = \frac{\partial}{\partial t} + \nabla\Phi\cdot\nabla$ is the material derivative.

In addition, the initial condition is usually based on the assumption that the free surface elevation is known together with the potential on the free surface, or

$$\eta(x, t=0) = \eta_I(x),\ \ \phi(x, y=\eta_I(x), t=0) = \phi_I(x), \tag{14}$$

where the expression of $\phi_I(x)$ and $\eta_I(x)$ need to be re-derived below due to the effect of a uniform incoming current.

2.2 *Solitary wave elevation and potential in a steady current*

In this section, we derive the potential and elevation of a solitary wave in a steady current by following the work of Friedrichs and Hyers (1954). Eq. (6) is rewritten as

$$\Phi = \phi(\theta, y) + Ux, \tag{15}$$

where $\theta = k(x-ct)$, k is wave number and c denotes phase velocity. Similarly, the wave elevation cab be expressed as

$$\eta(x,t) = \eta(\theta). \tag{16}$$

Therefore, the governing equation (7) and boundary conditions (8), (9) and (11) can be written as, respectively,

$$k^2\frac{\partial^2\phi}{\partial\theta^2} + \frac{\partial^2\phi}{\partial y^2} = 0, \tag{17}$$

$$-k(c-U)\frac{\partial\eta}{\partial\theta} + k^2\frac{\partial\phi}{\partial\theta}\frac{\partial\eta}{\partial\theta} - \frac{\partial\phi}{\partial y} = 0 \quad \text{on } S_f, \tag{18}$$

$$-k(c-U)\frac{\partial\phi}{\partial\theta} + \frac{1}{2}[k^2(\frac{\partial\phi}{\partial\theta})^2 + (\frac{\partial\phi}{\partial y})^2] + g\eta = 0 \quad \text{on } S_f, \tag{19}$$

$$\frac{\partial\phi}{\partial y} = 0 \quad \text{on } \ y = -h\ . \tag{20}$$

The initial conditions of the wave elevations are set to be

$$\eta(\theta=0) = A, \frac{\partial\eta}{\partial\theta}(\theta=0) = 0. \tag{21}$$

By employing the perturbation method in Friedrichs and Hyers (1954), the wave elevation η, velocity potential ϕ, phase velocity c and wave number k can be expanded into a series, respectively,

$$\eta = A\eta_0 + A^2\eta_1 + A^3\eta_2 + \cdots, \tag{22}$$

$$\phi = A^{1/2}(\phi_0 + A\phi_1 + A^2\phi_2 + \cdots), \tag{23}$$

195 $$c = c_0 + Ac_1 + A^2 c_2 + \cdots, \tag{24}$$

196 $$k = k_0(1 + Ak_1 + A^2 k_2 + \cdots), \tag{25}$$

197 where A is wave amplitude. The zero, first and second order equations can be obtained by
198 substituting Eqs. (23) and (25) into (17) and (20) and collecting the same order of both ends of
199 each equation:

200 Zero order:

201 $$\begin{cases} \dfrac{\partial^2 \phi_0}{\partial y^2} = 0 \quad \text{in } \forall \\ \dfrac{\partial \phi_0}{\partial y} = 0 \quad \text{on } y = -h. \end{cases} \tag{26}$$

202 First order:

203 $$\begin{cases} \dfrac{\partial^2 \phi_0}{\partial \psi^2} + \dfrac{\partial^2 \phi_1}{\partial y^2} = 0 \quad \text{in } \forall \\ \dfrac{\partial \phi_1}{\partial y} = 0 \quad \text{on } y = -h. \end{cases} \tag{27}$$

204 Second order:

205 $$\begin{cases} 2k_1 \dfrac{\partial^2 \phi_0}{\partial \psi^2} + \dfrac{\partial^2 \phi_1}{\partial \psi^2} + \dfrac{\partial^2 \phi_2}{\partial y^2} = 0 \quad \text{in } \forall \\ \dfrac{\partial \phi_2}{\partial y} = 0 \quad \text{on } y = -h. \end{cases} \tag{28}$$

206 In Eqs. (27) and (28), $\psi = A^{1/2}\theta / k_0$. Through Eqs. (26)~(28), we can obtain

207 $$\phi_0 = f_0, \tag{29}$$

208 $$\phi_1 = -\frac{1}{2}(y+h)^2 f_0'' + f_1, \tag{30}$$

209 $$\phi_2 = \frac{1}{24}(y+h)^4 f_0^{\mathrm{iv}} - \frac{1}{2}(y+h)^2 (2k_1 f_0'' + f_1'') + f_2. \tag{31}$$

210 It should be pointed out that f_0, f_1 and f_2 are only the function of ψ. Here, we may assume that
211 the velocity of current is of zero-order, or it has the same order with c_0. Then, the terms in free
212 surface boundary conditions (18) and (19) can be expanded to first order in a similar way:

213 $$\begin{cases} (c_0 - U)\ \eta_0' - h f_0'' = 0 \\ -(c_0 - U)\ f_0' + g\eta_0 = 0 \end{cases} \tag{32}$$

$$\begin{cases} -(c_0-U)\ \eta_1' + hf_1'' = [c_1 + k_1(c_0-U)]\eta_0' - f_0'\eta_0' - f_0''\eta_0 - 2k_1 hf_0'' + \dfrac{1}{6}h^3 f_0^{iv} \\ g\eta_1 - (c_0-U)\ f_1' = \dfrac{1}{2}f_0'^2 + [c_1 + k_1(c_0-U)]f_0' - \dfrac{1}{2}(c_0-U)h^2 f_0''' \end{cases} \tag{33}$$

By solving Eq. (31), we can obtain

$$c_0 = U + \sqrt{gh}\,, \tag{34}$$

$$f_0' = \sqrt{\frac{g}{h}}\eta_0\,, \tag{35}$$

and the following equation can be obtained by using Eq. (33)

$$\frac{1}{3}h^3\eta_0'' + \frac{3}{2}\eta_0^2 - \frac{2}{g}(c_0-U)c_1\eta_0 = 0\,, \tag{36}$$

and this equation is solved by using $\eta_0 = 1$ and $\eta_0' = 0$ at the wave crest according to Eq. (21) and we obtain

$$c_1 = \frac{1}{2}\sqrt{\frac{g}{h}}\,, \tag{37}$$

$$\eta_0 = \mathrm{sech}^2\sqrt{\frac{3A}{4h^3}}(x-ct)\,. \tag{38}$$

The wave elevation, potential and phase velocity can be obtained when it is considered to first order only

$$\eta = A\eta_0 = A\mathrm{sech}^2\sqrt{\frac{3A}{4h^3}}(x-ct)\,, \tag{39}$$

$$\phi = \sqrt{A}\phi_0 = \frac{2}{\sqrt{3}}h\sqrt{gA}\tanh\sqrt{\frac{3A}{4h^3}}(x-ct)\,, \tag{40}$$

$$c = c_0 + Ac_1 = U + \sqrt{gh}(1+\frac{1}{2}\frac{A}{h})\,. \tag{41}$$

The previous work by Cooker et al. (1997) and Zhou et al. (2016) have already indicated that the higher-order solutions will only have significant influence on the results when the amplitude A/h is very large. Our analysis below is restricted as $A/h \leq 0.4$ Thus, using the first-order approximation here is reasonable. Besides, it should be noticed that the initial position of the peak of the solitary wave is located at $x = 0$ in the above equations. Once it is located at $x = x_p$, the x in Eqs. (39) and (40) should be replaced as $x - x_p$. From Eqs. (39) ~ (41), we can know that once the solitary wave and uniform current coexist in a steady state, only the wave speed will be affected by the uniform current. The expressions of ϕ and η are in a same form as those of the cases without the current.

2.3 *Evaluation of hydrodynamic forces*

Once the velocity potential has been obtained through solving Eqs. (7), (10~14), the pressure in the fluid can be determined by Bernoulli equation

$$p = -\rho(\frac{\partial \phi}{\partial t} + U\frac{\partial \phi}{\partial x} + \frac{1}{2}|\nabla \phi|^2 + gy), \tag{42}$$

where ρ is the fluid density. The hydrodynamic force acting on the body can be expressed as

$$F_j = \iint_{S_b} pn_j ds, \tag{43}$$

where $(n_1, n_2, n_3) = (n_x, n_y, yn_x - xn_y)$, j=1,2 corresponding to the force (F_x, F_y) and j=3 to the moment M_z. In Eq. (43), the computation of the integration of $\partial\phi/\partial t$ may be a problem and the direct differencing of ϕ with time may cause the force history to be unsmooth. To overcome this difficulty, we extend the method developed by Wu (1998), which is used in cases without current to the present study on wave-current-body interactions.

In the fluid domain, the time derivative ϕ_t satisfies the Laplace equation

$$\nabla^2 \phi_t = 0. \tag{44}$$

On the fixed boundary it satisfies

$$\frac{\partial \phi_t}{\partial n} = 0. \tag{45}$$

On the free surface ϕ_t is given by the Bernoulli equation as

$$\phi_t = -gy - \frac{1}{2}\nabla\phi\nabla\phi - U\frac{\partial \phi}{\partial x}. \tag{46}$$

where $\vec{r}$ is the position vector of any point on the cylinder surface to the rotated centre. Eqs. (44) ~ (46) can be easily solved to obtain $\partial\phi/\partial t$.

3. Finite element discretization and numerical procedures

In the present simulations, we employed a finite element method with 8-node quadrilateral isoparametric element to calculate the velocity potential at each time step. Detailed finite element discretization can be found in Wang et al. (2011). The fourth-order Runge-Kutta method is adopted for updating the wave elevation and the potential on the free surface (Wang and Khoo, 2005; Wang et al., 2013; Wang et al., 2011). A B-spline method is used for remeshing and an energy method is for smoothing the free surface (Wang and Wu, 2006). A damping zone is placed at each end of the fluid domain to minimize the reflected wave. All these numerical techniques were also employed for simulating wave resonance by the oscillation of two cylinders in a steady current in Huang et al. (2022).

The velocity potential has been found through solving Eqs. (7), (10) – (14) based on the finite element method, the velocity on the free surface and cylinder surface can be obtained through differentiating the shape functions directly. The simulation is conducted in time domain by updating the velocity potential and wave elevation through Eqs. (12) and (13). The hydrodynamic force on the cylinder surface can also be obtained through Eq. (43).

4. Numerical results

4.1 Solitary waves propagate over a underwater and bottom-mounted cylinder

We first consider interactions between solitary waves and a bottom-mounted rectangular cylinder (see Fig. 1a). The calm water depth is h=1m. The cylinder has height d=0.6h and breadth b=40h, and its central line is at x=0. The case without current has been studied by Lin (2004) based on the viscous flow theory . In our simulations, the length of the computational domain is L=216h. The solitary wave amplitude is first chosen as A=0.1h and its peak is initially located at x_p=-50h. The nondimensional time is defined as $\tau = t/\sqrt{h/g}$. However, the situation becomes more complicated when there is a current because there are interactions between wave and current and also between current and cylinder besides wave-cylinder interaction.

Fig. 2 shows convergence tests for mesh and time interval. The test of waves is at x =-21h or x/h =-21with three current speeds U=-0.3, 0 & 0.3 m/s. Four meshes and two-time intervals are used to test the numerical convergence. The details are given in Table 1, in which n_f is the segment number along the free surface, n_d and n_h are the segments along the vertical faces of the cylinder and that along the artificial boundaries S_c, respectively, n_e and n_n are the total number of elements and nodes in the whole fluid domain respectively. The results for Cases 1 to 4 are given in Fig. 2. It can be seen that Case 2 are in very good agreement over the entire simulational time of $\tau = 200$ with Cases 3 and 4. The Case 1 with the coarse mesh, however, shows a clear difference at around $\tau = 150$ for U=-0.3 m/s (see Fig.2a) and during $\tau = 150$ and 200 for U=0 (see Fig.2b) with Cases 2, 3 and 4. Thus, these tests show that Case 2 can provide convergent results.

Table 1 Parameters of mesh schemes

	n_f	n_d	n_h	n_e	n_n	$d\tau$
Case 1	780	4	7	4580	15323	0.02
Case 2	1260	4	9	9900	32247	0.02
Case 3	1890	6	13	21330	67809	0.01
Case 4	2520	8	17	37080	116331	0.01

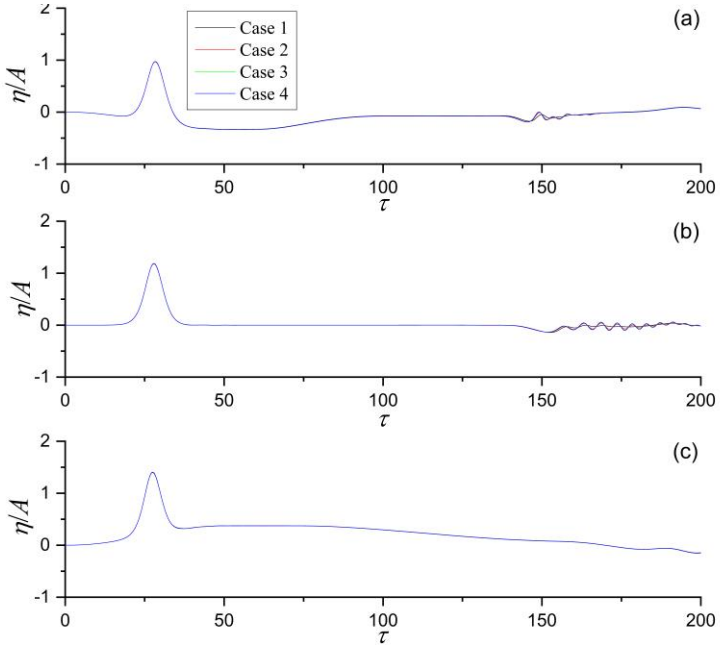

Fig. 2. Comparisons of waves at x/h=-21 between different meshes and time intervals at (a) U=-0.3m/s; (b) U=0; (c) U=0.3 m/s.

The wave profiles at τ=10, 40, 70 & 100 with U=-0.3, 0, & 0.3 m/s are given in Fig. 3. The waves at τ=10 is given in Fig.3a and it is seen that they have no clear difference since the time is short. However, with the development of time, it becomes clear at τ=40 in Fig. 3b. It can be seen from the figure that the wave surface outside cylinder within two regions of -55<x/h<-20 and 20<x/h<55 rises or sinks at U=0.3 & U=-0.3 m/s, and they then expand to the ranges of -80<x/h<-20 and 20<x/h<80 at τ=70 (see Fig. 3c) and to even wider range at τ=100 (see Fig. 3d). The wave surface elevates on the left region of the cylinder and sinks on the right region at U=0.3 m/s but it is opposite at U=-0.3 m/s, and this is because of the Doppler effect: the propagation of reflected wave within the left region is opposite to the current direction when U>0 and hence make the peak larger; On the contrary, the wave within the right region propagate to the positive x-direction, which is identical to the direction of current at U=0.3 m/s and hence cause a smaller peak. A similar explanation can be made for U=-0.3 m/*s*. Furthermore, the wave peak has been affected by the current. At τ=10, the peak at U=0.3 m/*s* is almost identical to those at U=0 & -0.3 m/*s*, and it then becomes larger than that at U=0 when τ=40. In contrast to this, the peak at U=-0.3 m/*s* is smaller than that at U=0. This is because of interactions between wave-current and the cylinder after the wave peaks pass over above the front of the cylinder. At τ=70 (see Fig. 3c), the wave at U=0.3 m/*s* propagates faster and pass over the whole cylinder and hence its peaks becomes the smallest and that at U=0, which is around above the second half of the cylinder, becomes the second smallest. In addition, a series of waves followed the main peak are generated and gradually evolve periodic waves when the waves have passed over the

whole cylinder especially for U=0.3 m/s since it propagates faster than those at U=-0.3 & 0 m/s when τ =100 (see Fig. 3d).

Fig. 4 shows wave histories at x/h=-29, 19 & 49 corresponding to Fig. 3. As discussed by Lin (2004) about wave reflection and transmission without current effect or U=0 m/s, there are two reflected waves in front of the cylinder, e.g. x/h=-29 due to interactions between the waves and the front and rear of the cylinder. When the wave propagates to some location above the cylinder and near its rear (x/h=19), the wave split into a number of solitons with decaying amplitude, and it then evolves into a soliton followed by a packet of small surface waves after they pass over the whole cylinder (x/h=49). All these can be seen in Fig. 4 and it shows a consistent result with the cases in Lin (2004). Similarity can be found in the cases of current at U=-0.3 & 0.3 m/s. However, the difference is clear between U=0 m/s and $U\neq$0 m/s. At x/h=-29, one main peak at around $\tau = 20$ followed by one secondary peak at around $\tau = 38$ can be observed (see Fig. 4a) at each speed, and they become larger as the increase of the current speed. On reason is that the wave is acted by the front of the cylinder and cause wave reflection and hence the second peaks appear at around $\tau = 38$, which has been explained by Lin (2004); The other is due to the Doppler effect of interactions between the reflected wave and the current, which cause both main and secondary peaks to increase as the increase of the current speed. It is also noticed that the secondary peak at U=-0.3 m/s is much smaller that those at U=0 & 0.3 m/s and its peak value is nearly equal to zero. In the case of the current at U=0.3 m/s, the wave is elevated until $\tau = 115$ by the current and nearly keep a constant at $\eta / A = 0.38$ between $\tau = 42$ and 84 and then gradually goes down. By contrast, the wave has a trough at around $\eta / A = -0.33$ between $\tau = 53$ and 71 at U=-0.3 m/s and it is then slowly ascended until $\tau = 140$.

Fig. 4b shows the wave at x/h=19, which is above the cylinder and is close to the rear corner of the cylinder. As discussed in the last paragraph, a series of solitons with decaying amplitude has already been generated at each speed and the main peak at U=0.3 m/s becomes the smallest due to current effect. When the wave continues to propagate to the right direction to the location x/h=49 shown in Fig. 4c, the solitons mentioned above, degenerate into a wave with soliton shape and a packet of small surface waves. Furthermore, it is also seen that the waves generally become larger at U=-0.3 m/s than those at U=0. On the contrary, the waves at U=0.3 m/s shows an opposite variation to that at U=-0.3 m/s and the solitons disappear more quickly. This is because of the Doppler effect of interaction between a wave and a current: the transmitted waves, which pass over the whole cylinder, propagate along the positive x-axis and it is identical to the current direction when U>0 and hence make the peak smaller and the situation is opposite to this when U<0.

The snap shots of wave profile from $\tau = 0$ to 100 with time interval $\Delta\tau = 1$ are given in Fig. 5, which exhibits wave evolution in space during a long period of time. It is shown from Fig. 5b that two reflected waves can be clearly seen when the solitary wave arrived at the front (x/h=-20) and real (x/h=20) of the cylinder at U=0 m/s, which has also been observed by Lin (2004). When the current exists, the first reflected wave by the front of cylinder (x/h=-20) can also be observed at U=-0.3 m/s (Fig. 5a) and U=0.3 m/s (Fig. 5c), the difference is that the latter is much clearer than the former and this can also be seen in Fig. 3. The second wave reflected by the rear of the cylinder (x/h=20) at U=-0.3 m/s is almost graphically unseen and this is because this wave become smaller when it is acted by the adverse current. However, it becomes significant at current speed U=0.3 m/s, which is oppose to the reflected wave, and it is even clear than that at U=0. Meanwhile, a series of waves including a soliton followed by surface waves at the three speeds propagate toward the x-direction after they pass over the rear corner of the cylinder can be seen in the figure. In addition, the wave's sink and rise can also be observed within the left region of the cylinder at U=-0.3 & 0.3 *m/s*, respectively.

In order to exhibit the wave nonlinearity, three incident wave amplitudes A/h=0.1,0.2 & 0.4 are used for calculating the waves at x/h=-21 and 19, which are close to the front and rear of the cylinder, respectively. The results are given in Figs. 6 and 7. It can be seen that the difference between the three nondimensional waves are evident at each current speed and location, which indicates the wave nonlinearity is clear. At x/h=-21, the nondimensional wave peak increases as the increase of A/h for U=-0.3 m/s. It then gradually reduces as A/h increases when the current speed is augmented to U=0 & 0.3 m/s and the trend of descent for latter is more evident. When the waves arrive at x/h=19 (see Fig. 7), the situation becomes very different due to sufficient interactions between the wave-current and the cylinder. The wave with single peak has already split into a soliton and a packet of surface waves with gradually decreasing amplitude one by one at each current speed. The nondimensional main peak definitely declines as the increase of A/h at each speed, which is even clearer than those at x/h=-21 in Fig. 6.

Fig. 8 give a comparison similar to Fig. 4 except that the initial draught is d/h =0.3. We compared the waves at x/h=-29 (see Fig.8a) with those at d/h=0.6 in Fig. 4a. It can be seen that the difference between three peaks at U=-0.3, 0 & 0.3 m/s is smaller than that in Fig. 4a. The three peaks become smaller when the waves arrive at x/h=19 (see Fig. 8b) at every speeds. Furthermore, the secondary peaks followed the main peak are much smaller at x/h=-29 and 19 (see Figs. 8a & 8b) than those at d/h =0.6. At x/h=49, the wave evolves into a soliton followed by a packet of travelling waves is not as evident as that at d/h=0.6 (see Fig. 8c and Fig. 4c). In summary, the current effect on the wave is relative weak and it is because the cylinder d/h =0.3

is far away from the free surface that that at d/h =0.6 and hence it causes weaker interaction between the wave-current and the cylinder.

Fig. 9 give another comparison similar to Fig. 4 except that the cylinder breadth is b/h =2. Compared with Fig. 4, the magnitudes of three wave peaks at three locations and U=-0.3, 0 & 0.3 m/s have slight difference and not as clear as those at b/h=40. This is because it takes longer times when the wave passes over the cylinder at b/h=40, which causes a more sufficient wave-current-body interaction.

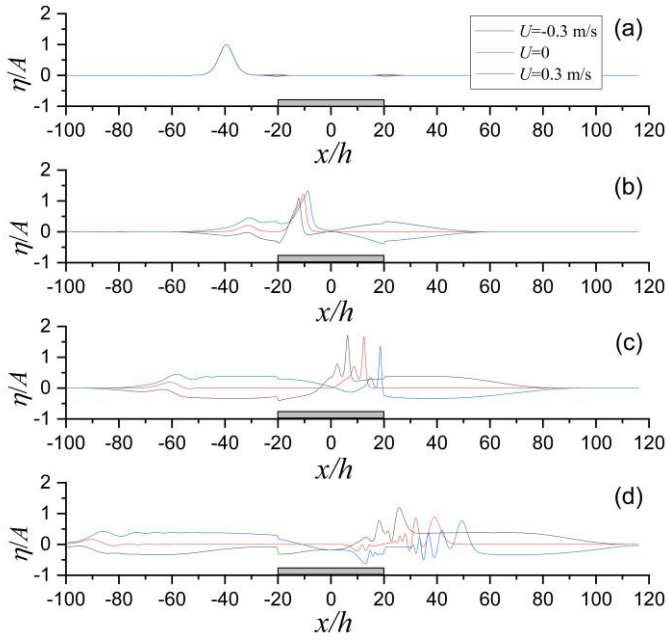

Fig. 3. (a) wave profiles at (a) τ=10; (b) τ=40; (c) τ=70 (d) τ=100 at A/h=0.1.

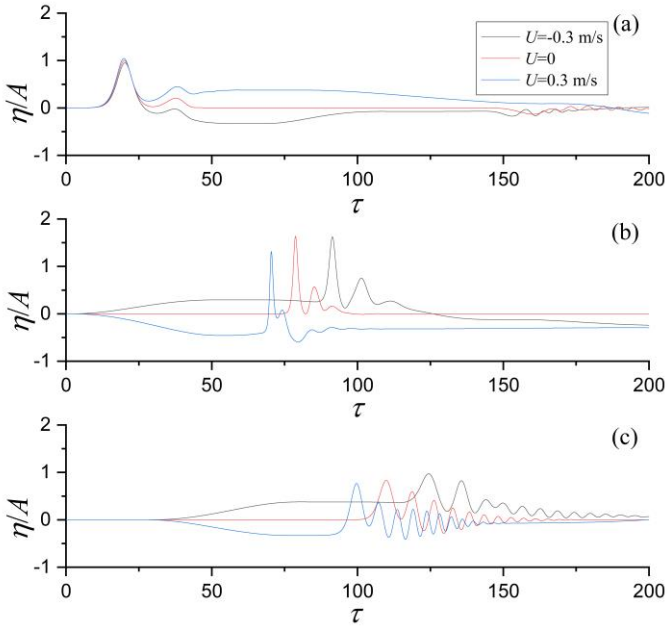

Fig. 4. Wave histories at d/h=0.6 (a) x/h=-29; (b) x/h=19; (c) x/h=49.

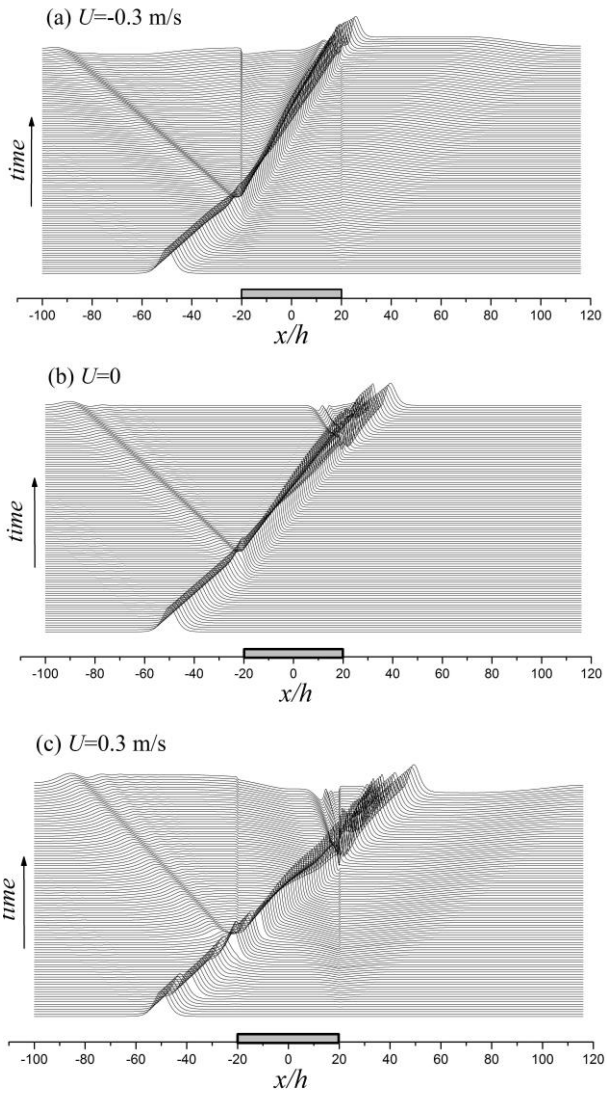

Fig. 5. Snap shots of wave profile from $\tau = 0$ to 100 with time interval $\Delta\tau = 1$ and A/h=0.1.

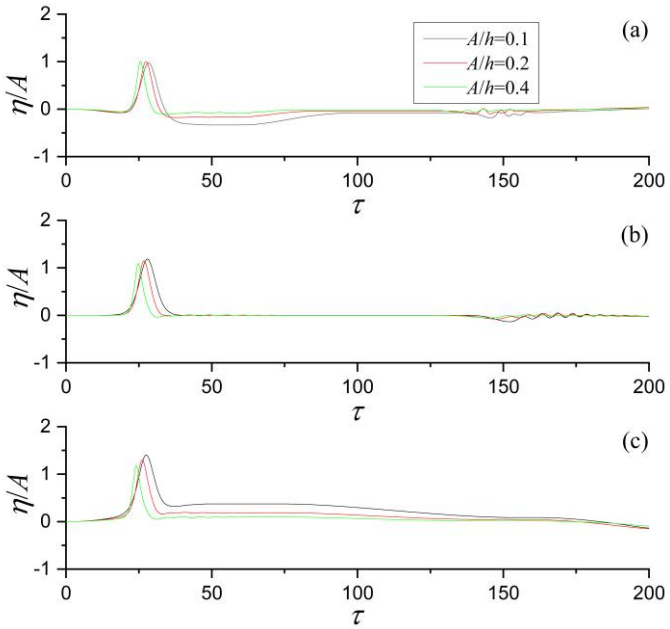

Fig. 6. Wave histories at x/h=-21; (a) U=-0.3m/s; (b) U=0; (c) U=0.3 m/s.

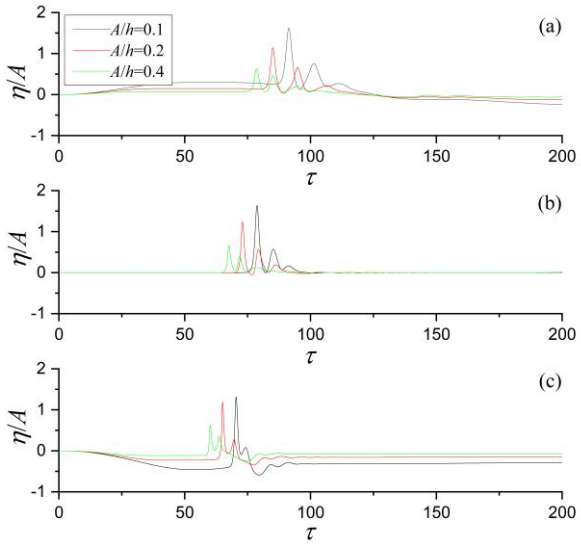

Fig. 7. Wave histories at x/h=19; (a) U=-0.3 m/s; (b) U=0; (c) U=0.3 m/s.

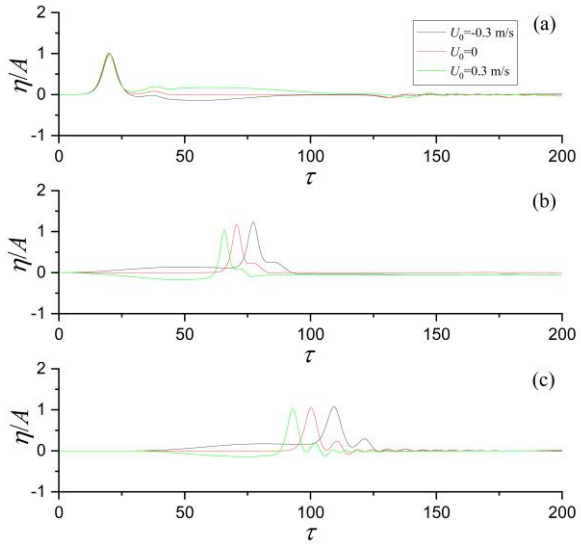

Fig. 8. Wave histories at d/h =0.3; (a) x/h=-29; (b) x/h=19; (c) x/h=49.

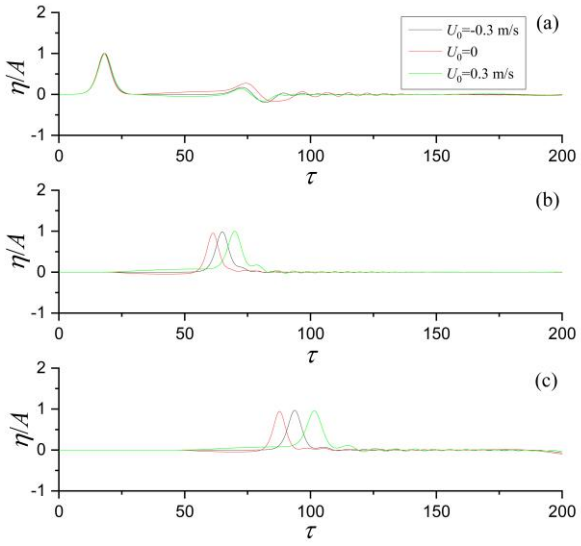

Fig. 9. Wave histories at d/h =0.6 and b/h=2; (a) x/h=-29; (b) x/h=19; (c) x/h=49.

4.2 Interactions between a solitary wave and a rectangular cylinder in a current

Sun et al. (2015) simulated interactions between a solitary wave and a rectangular cylinder without current effect. In this section, we extend the work of Sun et al. (2015) to the situation with a steady current, which is related to interactions of a solitary wave with a ship advancing in offshore area. It should be noted that the present numerical method is already verified by comparing with the results without the current in Sun et al. (2015) by setting $U = 0$ here. We consider a cylinder with breadth $b=h$ and initial draught $d=0.5h$ and its central line is located at $x=0$ (see Fig. 1b). The length of fluid domain on the left and right sides is $L_{left}=L_{right}=120h$ and the initial wave peak is at $x_p=-L_{left}/2$. In the simulation, $h=1m$. We calculate waves and hydrodynamic forces on the cylinder. To enable the interactions between the cylinder and current to develop smoothly, a modulation function $M(t)$ is applied to let the current gradually increase

$$U_0' = M(t)U_0 \ ,$$

where

$$M(t) = \begin{cases} \frac{1}{2}[1-\cos(\frac{\pi t}{T})] & t < T \\ 1 & t \geq T \end{cases}$$

and T is period of time. Fig. 10 shows the wave histories at the left side of the cylinder with current-cylinder interactions only at F_n=0.04, 0.08 & 0.16. Each wave changes quickly in the beginning and finally reaches to a constant. We chose T as 4.79 (sec), which corresponds to the nondimensional time τ=15, at which each wave has already been stable.

Fig. 11 shows the wave histories at the left and right sides of the cylinder at A/h=0.09 and five different Froude numbers F_n=-0.16, -0.08, 0, 0.08 & 0.16 are used, where F_n is the Froude number and it is defined as $F_n = U/\sqrt{gb}$. It can be seen that the main peaks of the solitary waves at both left and right sides increase as the increase of F_n and the former is clearer, which is similar to a periodic wave diffraction by the cylinder. The wave shape around the peak is sharper at larger F_n and hence has stronger nonlinearity. It is also interesting to see that the waves at the left and right sides finally evolves into a steady periodic wave with large constant peaks and troughs at F_n=0.16 and -0.16, respectively, and the peak of the periodic wave is even larger than that of the solitary wave. However, no clear periodic wave appears at F_n=-0.08, 0 & 0.08.

Fig. 12 shows wave histories at a large amplitude A/h=0.36. Similar to that at A/h=0.09, the main peak at each side also increases as F_n increase but those at the left side are even clearer than those at A/h=0.09 and hence has even stronger nonlinearity at larger F_n. At F_n=0.16 and -

0.16, the waves at left and right sides also become stable with constant peak and trough after a shorter period of time than that at A/h=0.09. All these exhibit that the solitary wave has stronger nonlinearity at larger Froude numbers and also indicate that a clearly periodic wave can more easily appear at large absolute value of Froude number $|F_n|$.

We give further comparisons of waves at both sides with three incident wave amplitudes A/h=0.09, 0.18 & 0.36 and three Froude numbers F_n=-0.16, 0 & 0.16 are used. The result is shown in Fig. 13. The case without current or F_n=0 has been analyzed by Sun et al. (2015) and they found that the nondimensional peak and trough of the solitary wave at the left side increase as the increase of incident wave amplitude. As expected, they also increase as the amplitude increases at F_n=-0.16 & 0.16. The peaks at the left side increases 28.1%, 14.6% & 18.1% from A/h=0.09 to 0.18 at F_n=-0.16, 0 & 0.16, respectively, and they are 40.3%, 37.1% & 44.0%, respectively from A/h=0.09 to 0.36. The discrepancy between the three amplitudes becomes larger at larger Froude numbers, which indicates sharper peaks or troughs at larger amplitudes and hence exhibit stronger nonlinearity. The nondimensional peak of the solitary wave at the right side, however, shows a reverse variation with the incident wave amplitude at each Froude number, and it can also be seen that the peak values have no evident difference between the three Froude numbers. Furthermore, it has already been noticed In Figs. 11a and 12a that the left wave at F_n=0.16 and the right wave at F_n=-0.16 finally evolve into periodic waves with larger constant peak and trough. Actually, the left wave at F_n=-0.16 (Fig. 13a) and the right wave at F_n=0.16 (Fig. 13f) also trend to become periodic and stable but with much smaller peaks and troughs at all incident wave amplitudes. Figs. 13b & 13e gives comparisons of right wave at F_n=-0.16 and the left at F_n=0.16 to show the variation from A/h=0.09 to 0.18 and to 0.36. It is clearly seen that the nondimensional peaks of periodic waves at both sides decline as the increase of incident wave amplitude.

The corresponding hydrodynamic force excluding the initial buoyancy are shown in Fig. 14, in which F_x and F_y expresses the force components in the horizontal and vertical directions, respectively. It can be seen that the variations of the force peaks in the horizontal and vertical directions with the amplitude at each Froude number are similar to the wave at the left and right sides, respectively. The forces in both directions also become periodic and stable at $|F_n| = 0.16$ after a period of time (see Fig. 14a, b, e & f). Furthermore, the force components in both horizontal and vertical directions also finally beocme periodic after a period of time. It is noticed the part of the vertical force component after the peaks at $|F_n| = 0.16$ (see Fig. 14b & f) move to the negative y-direction as the decrease of the amplitude. The main reason is that the current

causes a negative force in the vertical direction and the vertical force is dominated by the current at smaller amplitudes but by the wave at larger amplitudes.

The wave profiles at τ=40 and 60 are given in Fig. 15. As mentioned in Sun et al. (2015), there are wave transmission and reflection when a solitary wave acted a cylinder on free surface. The transmitted wave can keep its shape but with a smaller peak, and the reflected wave is a travelling wave with decaying peaks and troughs one by one. We now consider the effect of the current on the transmitted and reflected waves. Three current speeds at F_n=-0.16, 0 & 0.16 are used in the simulation and the incident wave amplitude is A/h=0.18. It is seen from Fig. 15 that the peaks of the transmitted waves have vey little difference at F_n=-0.16, 0 & 0.16 for both τ =40 and 60, and their peaks are clearly smaller than the incident wave amplitude. The reflected waves, however, obviously increase in all peaks and troughs as the Froude number increases. At τ=40, the first peak at F_n=-0.16 is 28.1% smaller than that at F_n=0 but it is 36.9% larger at F_n=0.16 than that at F_n=0. For the troughs, they are 27.4% and 32.4%, respectively. This is because of the Doppler effect, which is similar to that in the underwater and bottom-mounted cylinder case mentioned above.

Fig. 16 shows the wave run-ups denoted by R at the left and right sides as functions of the Froude number. It can be seen that the nondimensional wave run-up at the left side nearly linearly increases with the increase of F_n at every A/h. The run-ups at the right side, however, are less affected by the current and all of them are smaller than those at the left, which is consistent with the results mentioned above.

The peaks and troughs of the hydrodynamic force corresponding to Fig. 16 are plotted in Fig. 17, in which *max* and *min* denote the force peak and trough, respectively, and hereinafter for other figures. It is seen that the force peaks and troughs in the x-direction also nearly linearly increase as F_n increases at every A/h and they also enhance when A/h becomes larger at every F_n. The vertical forces show more complicate variations. The peak generally decreases as F_n increases at each A/h. It becomes smaller as A/h increases at smaller F_n and its change is opposite in larger F_n. The trough decreases as F_n increases at smaller F_n and then show a trend of increase at larger F_n. Based on the potential flow theory, there is no hydrodynamic force in the horizontal direction but a negative force exists in the vertical if a current only acts on a symmetric body in calm water surface. Thus, the current has smaller effect on the composite horizontal force acted by both wave and current. However, its effect is more important on the vertical force and hence may cause relatively complicate variation with the change of the Froude number.

Fig. 18 shows wave profiles from $\tau = 0$ to $\tau = 80$ with time interval $\Delta\tau = 1$ at A/h=0.36, which exhibits the process of wave evolvement in space over a long period of time. The development of transmitted and reflected waves with time can be clearly seen. In particular, the reflected waves within the left region of the cylinder become more evident as the increase of F_n.

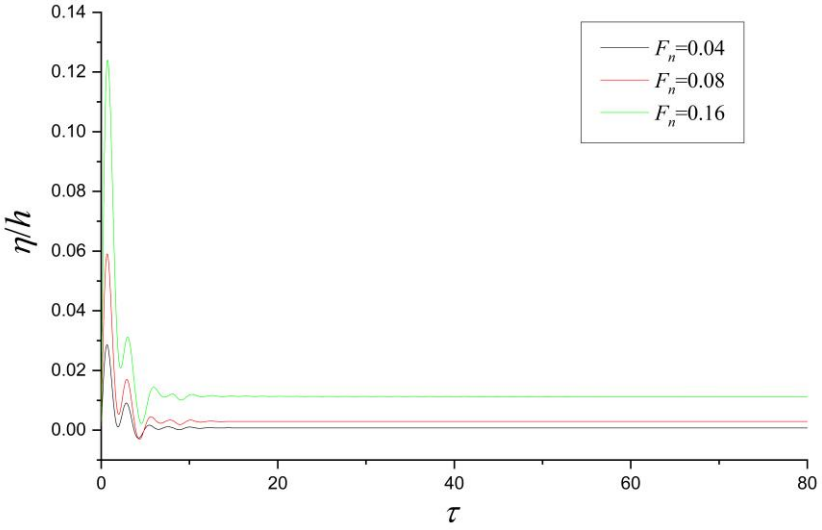

Fig. 10. Waves at the left side of cylinder due to current.

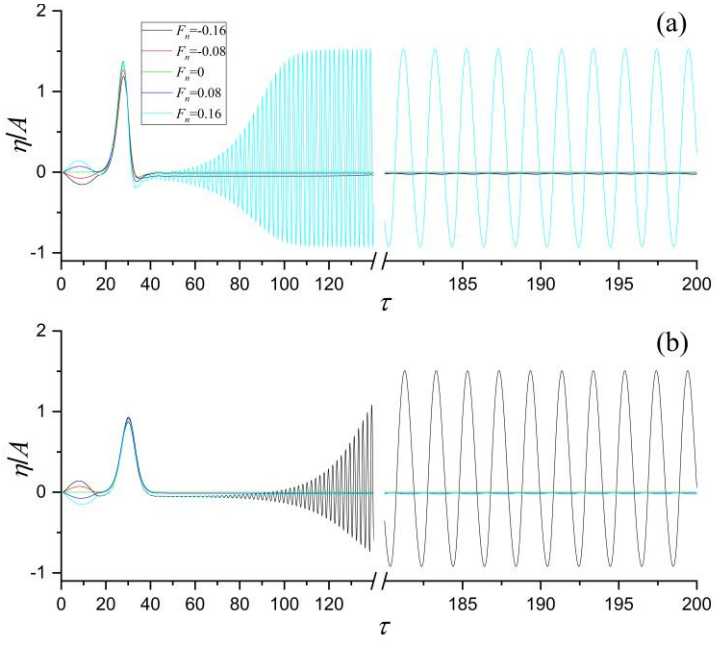

Fig. 11. Histories of waves at A/h=0.09; (a) left side; (b) right side.

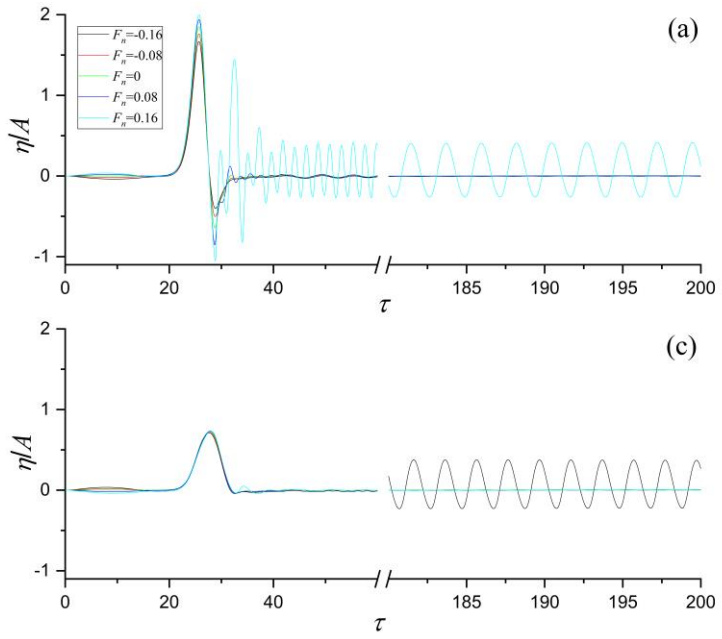

Fig. 12. Histories of waves at *A/h*=0.36; (a) left side; (b) right side.

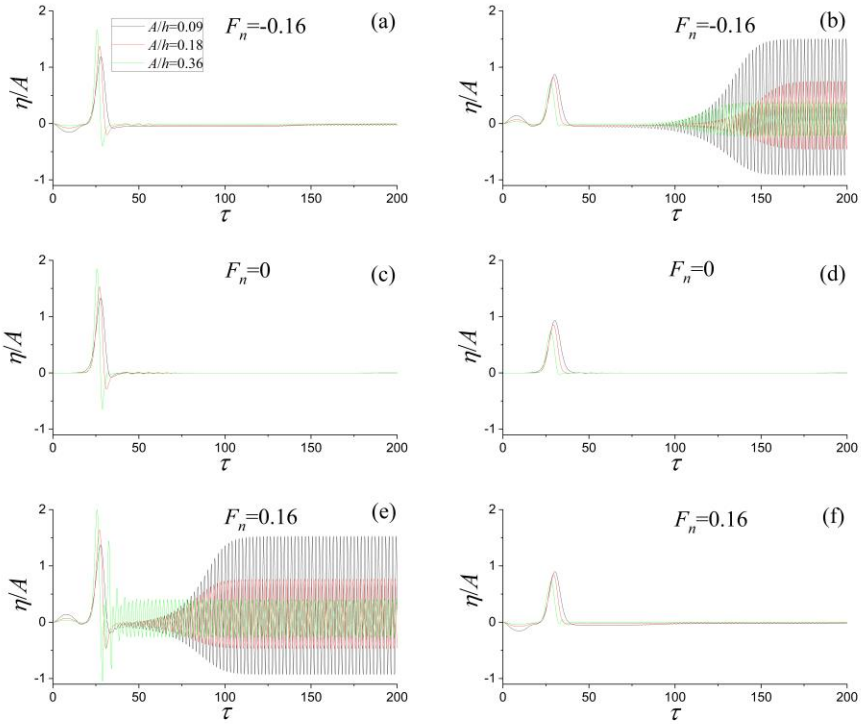

Fig. 13. Histories of waves at both sides of cylinder 1; (a), (c) & (e) left side; (b), (d) & (f) right side.

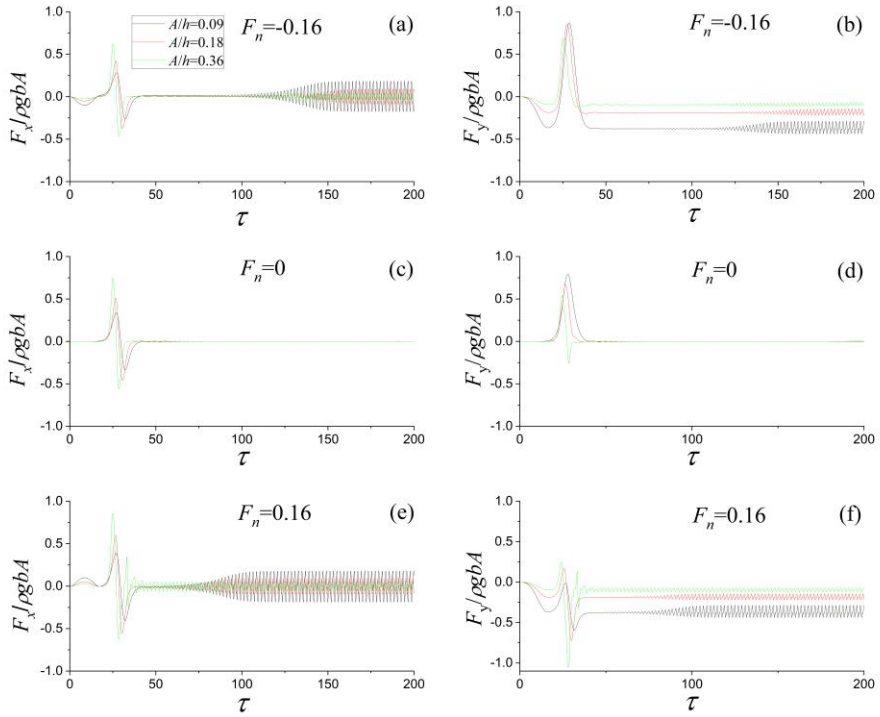

Fig. 14. Histories of hydrodynamic forces on the cylinder.

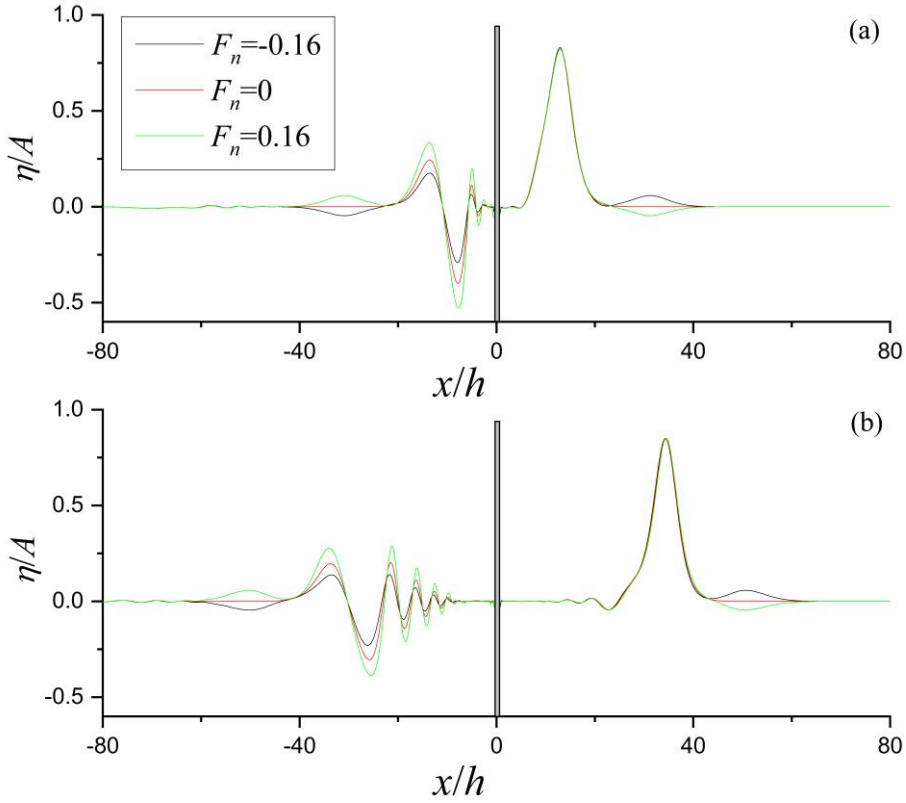

Fig. 15. Wave profiles at (a) $\tau = 40$; (b) $\tau = 60$.

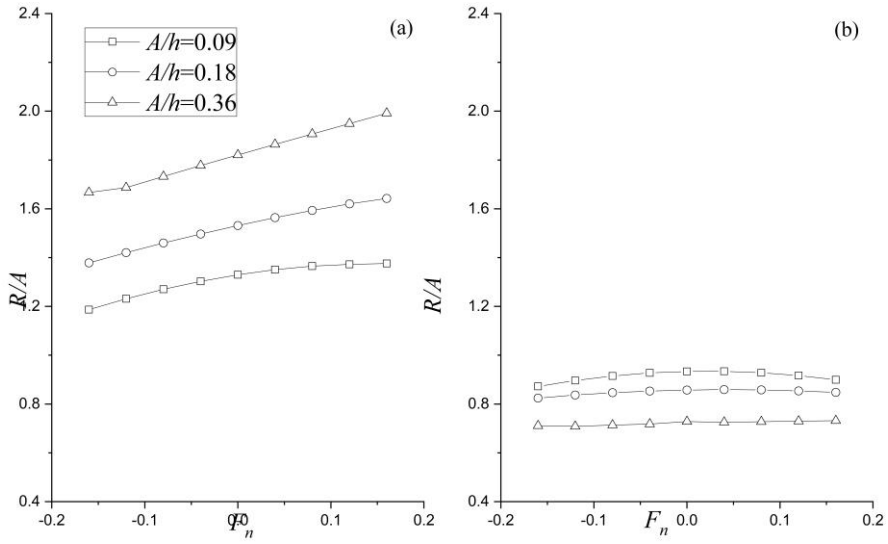

557

558 **Fig. 16.** Wave run-ups versus the Froude number; (a) left side; (b) right side.

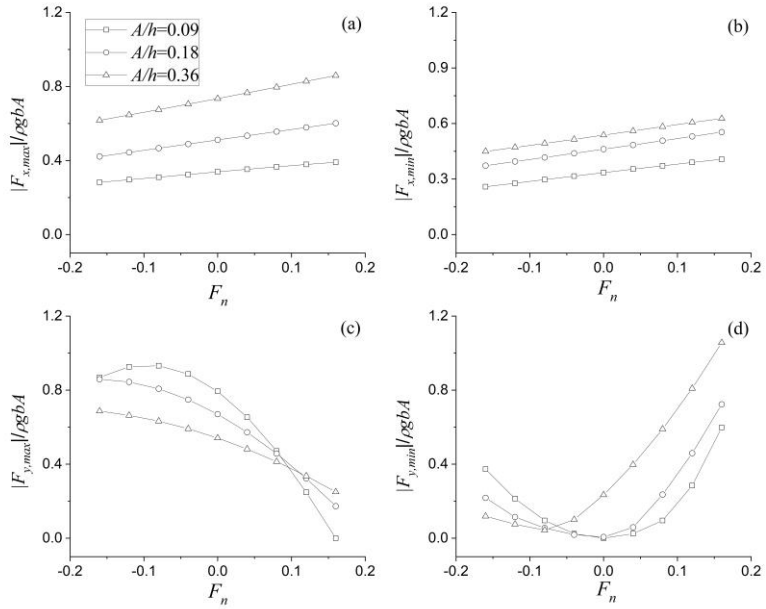

559

560 **Fig. 17.** Force peak and trough versus Froude number

561

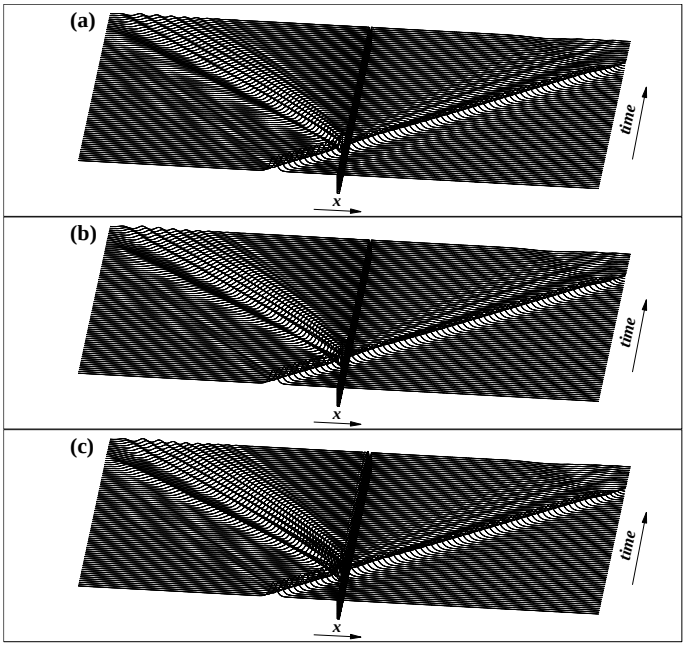

Fig. 18. Snap shots of wave profiles from $\tau = 0$ to $\tau = 80$ with time interval $\Delta\tau = 1$ at A/h=0.36; (a) F_n=-0.16; (b) F_n=0; (c) F_n=0.16.

4.3 Interactions between a solitary wave and twin rectangular cylinders in a current

Following the work of Sun et al. (2015), we further study interactions between solitary waves and a twin-cylinder but with considering the existence of a steady current. The dimension of each cylinder is identical to the single cylinder mentioned-above. The spacing between central lines of both cylinders is denoted as l_c, and the centerlines of cylinders are located at x=0 and l_c, respectively. Fig. 19 gives wave run-ups at l_c/b=4 with three incident wave amplitudes A/h=0.09, 0.18 & 0.36. Compared with the single cylinder cases in Fig. 16a, it seems that the run-ups for the left cylinder (cylinder 1) are slightly affected by the existence of the right cylinder (cylinder 2). The run-ups for cylinder 2 are relatively smaller than those for cylinder 1. Just like the situation in the single isolated cylinder cases given in Fig. 16, the run-ups of the solitary waves gradually increase and decrease as F_n increases at the left and right sides of both cylinders, respectively, at every A/h, but they have little change at the right sides of both cylinders. A difference with the single isolated cylinder case is that the wave peaks at the left side of cylinder 2 decline as the increase of A/h at every F_n (see Fig. 13c), which is similar to that at the right side of each cylinder.

Fig. 20 shows the results of wave histories and only cylinder 1 is given because the wave peaks around it are larger. Compared with the single cylinder cases in Fig. 13, the wave interference is clearly seen. At the left side, the waves are a little affected by the interference. However, the main peaks of solitary waves and the peaks and troughs of the periodic waves seem to not be nearly identical to those in the single isolated cylinder cases through comparing Fig.20a,

c &e and Fig.13a,c &e; at the right side (see Figs. 20b,d &f), they are very different from those in Figs. 13b, d & f due to the interference by the right cylinder.

Figs. 21 and 22 show the maximum and minimum hydrodynamic forces on both cylinders versus the Froude number. The horizontal components on both cylinders always increase as F_n and A/h, and the difference between them is that it is much clearer for cylinder 1. The situation of vertical components is similar to that in the single cylinder cases.

Fig. 23 shows that the wave run-up versus the spacing l_c/b at A/h=0.18. It is seen that the wave peaks at different l_c/b are generally larger at larger F_n except those at the right of cylinder 2. At smaller l_c/b, The wave peak at each Froude number grow up or down more quickly as the change of l_c/b especially for those at the right side of cylinder 1 and left side of cylinder 2 (see Fig. 23b, c), which means smaller spacing has more influence on the waves peaks at every F_n; With l_c/b continuing to increase, they almost reach constants at every F_n. It is also noticed that the waves at the right side have very little difference at larger l_c/b for cylinder 1 and all l_c/b for cylinder 2.

Fig. 24 shows the hydrodynamic forces corresponding to Fig. 23. Similar to the wave runups in Fig. 23, the effect of the spacing on the forces is also clear within smaller l_c/b. The maximum and minimum values of horizontal force generally increase as l_c/b in the beginning and finally reach a constant at each F_n, and they become larger at larger F_n within all l_c/b. The maximum of vertical force also become a constant at each F_n when l_c/b is large enough. However, it is decreases as F_n increases at every l_c/b.

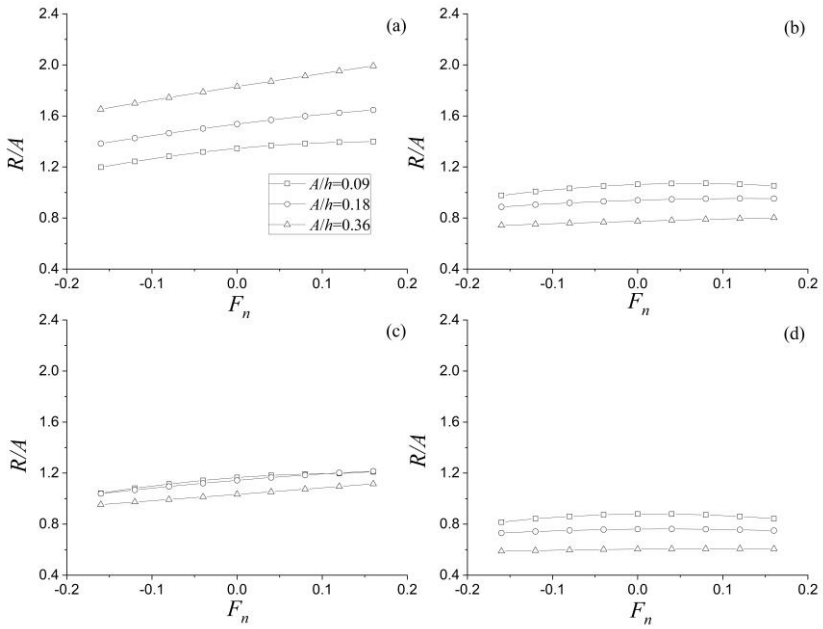

Fig. 19. Wave run-ups at the (a) left side of cylinder 1; (b) right side of cylinder 1; (c) left side of cylinder 2; (d) right side of cylinder 2.

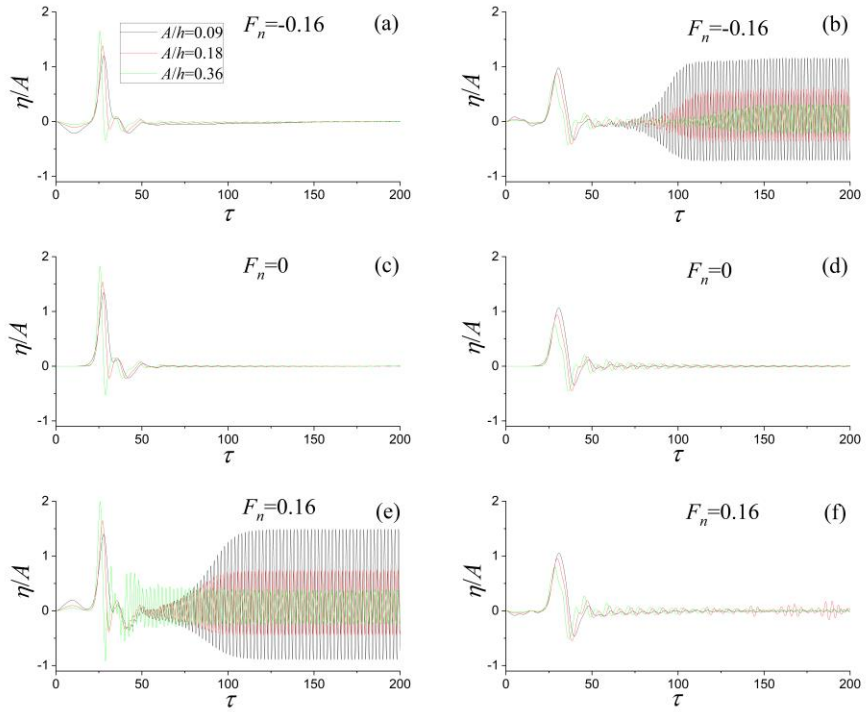

612
613 **Fig. 20.** Histories of waves at both sides of cylinder 1; (a), (c) & (e) left side; (b), (d) & (f) right side.
614
615

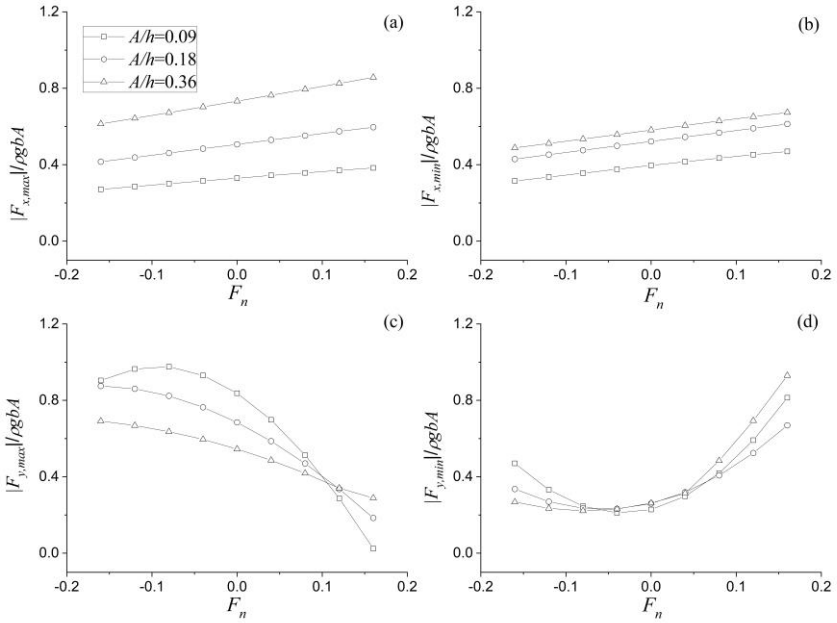

616
617 **Fig. 21.** Maximum and minimum forces on cylinder 1 versus Froude number
618

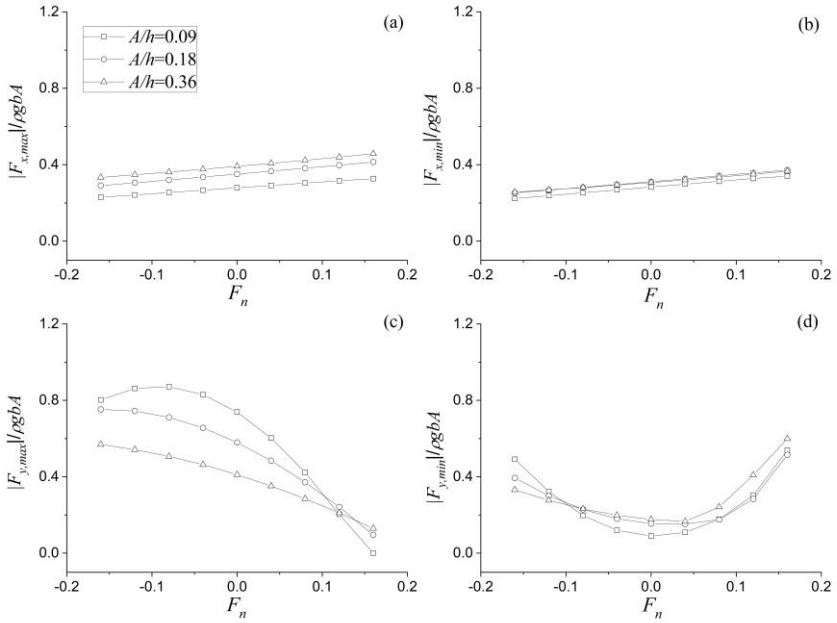

Fig. 22. Maximum and minimum forces on cylinder 2 versus Froude number

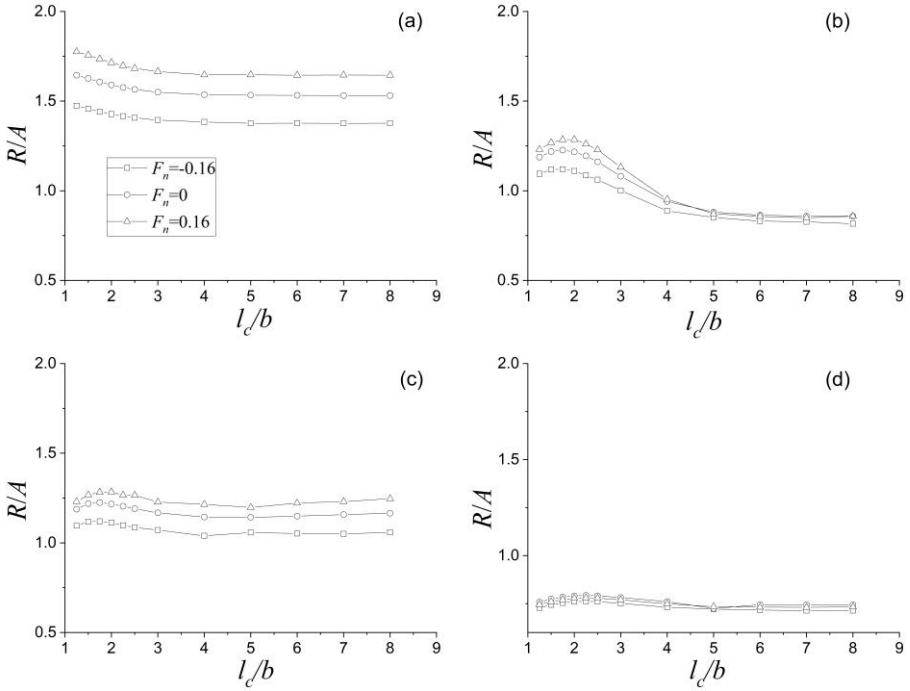

Fig. 23. Wave peak versus cylinder spacing at A/h=0.18; (a) left of cylinder 1; (b) right of cylinder 1; (c) left of cylinder 2; (d) right of cylinder 2.

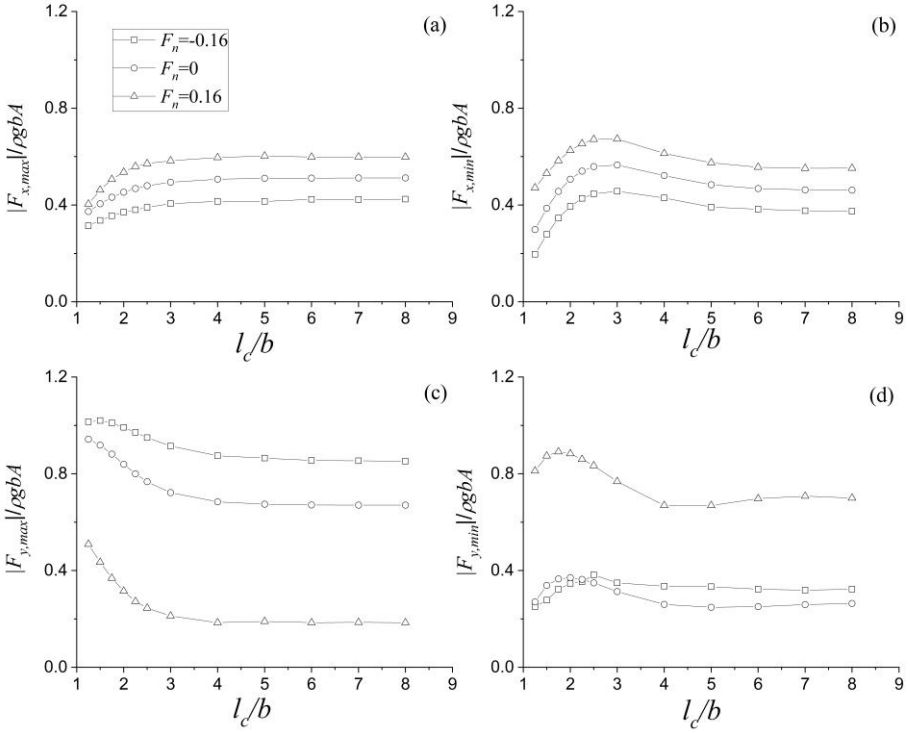

Fig. 24. Maximum and minimum forces on cylinder 1 versus cylinder spacing at A/h=0.18.

5. Conclusions

A higher order finite element method with a mesh of 8-node quadrilateral isoperimetric elements has been utilized to analyze the fully nonlinear interactions between solitary waves and structures in a steady current. The velocity potential at each time step is obtained through solving linear equation system based on an iteration method. The fourth order Runge-Kutta method is used to update the wave elevation and potential on the free surface at each time step. The radiation condition is imposed through placing a damping zone at one or both ends of the tank. The conclusion of this study is summarized as below:

Solitary wave propagation over an underwater rectangular cylinder in a current has been simulated. It is found that the following current cause the wave level in the upstream zone or the left range of the cylinder to elevate and that in the downstream zone or the right range to sink, and it is just the opposite for the adverse current. Furthermore, the effect of current on wave reflection and transmission has been investigated. Both the first reflection by the front of cylinder and the second reflection by its rear are more serious in the case of the following current, which causes the main peak and the travelling wave peaks to increase; the peak of transmitted wave is, however, less affected by the current but with faster propagation as the increase of current speed. In addition, the effect of cylinder breadth and height on waves and forces at different speeds has also been investigated. The simulations show that they can affect the wave diffraction and

transmission and cause the maximum of waves and forces to increase or decrease clearly and regularly.

Further simulations of solitary wave interactions with a single rectangular cylinder on free surface in a steady current have been made. The features of wave diffraction and transmission have been studied. It is found that a packet of periodic waves follows a soliton at each side of the cylinder and the periodic waves become clearly stable with constant peak and trough when the absolute value of the Froude number become large enough. Also, the peak of the periodic wave at the upstream side is much larger than that at the downstream. The nondimensional peaks of the soliton and the periodic waves due to the wave diffraction increase with the increase of the incident wave amplitude and Froude number or current speed; the transmitted wave peak is, however, a little affected by the Froude number. The peak and trough of the horizontal component of force generally increase as the Froude number increases at each incident wave amplitude but the vertical is not necessary.

Solitary waves interacting with a twin-cylinder has also been made. The effect due to current, incident wave amplitude and cylinder spacing on the wave and force is discussed in detail, and it is shown that the interference is more serious in larger currents, lager incident wave amplitudes and in smaller spacing.

In all the cases mentioned above, the nonlinearity at different incident wave amplitudes has also been studied. The numerical simulation exhibits the nonlinear features of wave and the hydrodynamic force at different current speeds and it is found that it is clear.

Acknowledgement

This work was supported by National Natural Science Foundation of China (Grant No. 51679096), to which the authors are most grateful. The first author is grateful to Lloyd's Register Foundation and China Scholarship Council for sponsoring his PhD study.

References

Cao, Y., Beck, R.F., Schultz, W.W., 1993. Numerical computations of two‐dimensional solitary waves generated by moving disturbances. International journal for numerical methods in fluids 17 (10), 905-920.

687 Carrier, G.F., Greenspan, H.P., 1958. Water waves of finite amplitude on a sloping beach.
688 Journal of Fluid Mechanics 4 (1), 97-109.
689 Celebi, M.S., 2001. Nonlinear transient wave–body interactions in steady uniform currents.
690 Computer methods in applied mechanics and engineering 190 (39), 5149-5172.
691 Chambarel, J., Kharif, C., Touboul, J., 2009. Head-on collision of two solitary waves and
692 residual falling jet formation. Nonlinear Processes in Geophysics 16 (1), 111-122.
693 Chen, Y., Kharif, C., Yang, J., Hsu, H., Touboul, J., Chambarel, J., 2015. An experimental study
694 of steep solitary wave reflection at a vertical wall. European Journal of Mechanics-B/Fluids
695 49, 20-28.
696 Cheng, Y., Li, G., Ji, C., Zhai, G., 2020. Solitary wave slamming on an Oscillating Wave Surge
697 Converter over varying topography in the presence of collinear currents. Physics of Fluids
698 32 (4), 047102.
699 Chian, C., Ertekin, R., 1992. Diffraction of solitary waves by submerged horizontal cylinders.
700 Wave Motion 15 (2), 121-142.
701 Cooker, M.J., Weidman, P.D., Bale, D.S., 1997. Reflection of a high-amplitude solitary wave at
702 a vertical wall. Journal of Fluid Mechanics 342, 141-158.
703 Friedrichs, K.O., Hyers, D., 1954. The existence of solitary waves. Communications on Pure
704 and Applied Mathematics 7 (3), 517-550.
705 Huang, H., Yang, Y., Zhu, R., Wang, C., 2022. Nonlinear wave resonance due to oscillations of
706 twin cylinders in a uniform current. Applied ocean research 121, 103096.
707 Isaacson, M., 1982. Nonlinear-wave effects on fixed and floating bodies. Journal of Fluid
708 Mechanics 120, 267-281.
709 Kim, S.K., Liu, P.L.-F., Liggett, J.A., 1983. Boundary integral equation solutions for solitary
710 wave generation, propagation and run-up. Coastal Engineering 7 (4), 299-317.
711 Knowles, J., Yeh, H., 2018. On shoaling of solitary waves. Journal of Fluid Mechanics 848,
712 1073-1097.
713 Kodama, Y., Yeh, H., 2016. The KP theory and Mach reflection. Journal of Fluid Mechanics
714 800, 766-786.
715 Lin, P., 2004. A numerical study of solitary wave interaction with rectangular obstacles. Coastal
716 Engineering 51 (1), 35-51.
717 Maiti, S., Sen, D., 1999. Computation of solitary waves during propagation and runup on a slope.
718 Ocean Engineering 26 (11), 1063-1083.
719 Miles, J.W., 1977. Obliquely interacting solitary waves. Journal of Fluid Mechanics 79 (1), 157-
720 169.
721 Mirie, R.M., Su, C., 1982. Collisions between two solitary waves. Part 2. A numerical study.
722 Journal of Fluid Mechanics 115, 475-492.

Ryu, S., Kim, M., Lynett, P.J., 2003. Fully nonlinear wave-current interactions and kinematics by a BEM-based numerical wave tank. Computational mechanics 32 (4), 336-346.

Seabra-Santos, F.J., Renouard, D.P., Temperville, A.M., 1987. Numerical and experimental study of the transformation of a solitary wave over a shelf or isolated obstacle. Journal of Fluid Mechanics 176, 117-134.

Sibley, P., Coates, L., Arumugam, K., 1982. Solitary wave forces on horizontal cylinders. Applied ocean research 4 (2), 113-117.

Su, C., Mirie, R.M., 1980. On head-on collisions between two solitary waves. Journal of Fluid Mechanics 98 (3), 509-525.

Sun, J., Wang, C., Wu, G., Khoo, B., 2015. Fully nonlinear simulations of interactions between solitary waves and structures based on the finite element method. Ocean Engineering 108, 202-215.

Synolakis, C.E., 1987. The runup of solitary waves. Journal of Fluid Mechanics 185, 523-545.

Tanaka, M., 1993. Mach reflection of a large-amplitude solitary wave. Journal of Fluid Mechanics 248, 637-661.

Wang, C., Khoo, B., 2005. Finite element analysis of two-dimensional nonlinear sloshing problems in random excitations. Ocean Engineering 32 (2), 107-133.

Wang, C., Meng, Q., Huang, H., Khoo, B., 2013. Finite element analysis of nonlinear wave resonance by multiple cylinders in vertical motions. Computers & fluids 88, 557-568.

Wang, C., Wu, G., 2006. An unstructured-mesh-based finite element simulation of wave interactions with non-wall-sided bodies. Journal of Fluids and Structures 22 (4), 441-461.

Wang, C., Wu, G., Khoo, B., 2011. Fully nonlinear simulation of resonant motion of liquid confined between floating structures. Computers & fluids 44 (1), 89-101.

Wang, J., Ma, Q., Yan, S., 2018. A fully nonlinear numerical method for modeling wave–current interactions. Journal of Computational Physics 369, 173-190.

Wang, K.-H., Jiang, L., 1993. Solitary wave interactions with an array of two vertical cylinders. Applied ocean research 15 (6), 337-350.

Wang, K.-H., Wu, T.Y., Yates, G.T., 1992. Three-dimensional scattering of solitary waves by vertical cylinder. Journal of waterway, port, coastal, and ocean engineering 118 (5), 551-566.

Wu, G., 1998. Hydrodynamic force on a rigid body during impact with liquid. Journal of Fluids and Structures 12 (5), 549-559.

Yates, G., Wang, K.-H., 1994. Solitary wave scattering by a vertical cylinder: experimental study, The Fourth International Offshore and Polar Engineering Conference. OnePetro.

Zhang, J., Zheng, J., Jeng, D.-S., Guo, Y., 2015. Numerical simulation of solitary-wave propagation over a steady current. Journal of waterway, port, coastal, and ocean engineering 141 (3), 04014041.

760 Zhao, M., Cheng, L., Teng, B., 2007. Numerical simulation of solitary wave scattering by a
761 circular cylinder array. Ocean Engineering 34 (3-4), 489-499.
762 Zhou, B., Wu, G., Meng, Q., 2016. Interactions of fully nonlinear solitary wave with a freely
763 floating vertical cylinder. Engineering Analysis with Boundary Elements 69, 119-131.
764 Zhou, B., Wu, G., Teng, B., 2015. Fully nonlinear wave interaction with freely floating non-
765 wall-sided structures. Engineering Analysis with Boundary Elements 50, 117-132.
766